www.ijarp.com ISSN 2456-9992 Page: 01-21

International Journal Advanced Research Publications

Research Article

Volume: 02
Issue: 07

# MICROSTRUCTURAL AND CRYSTALLOGRAPHIC CHARACTERIZATION OF HIGH-DENSITY POLYETHYLENE/ALUMINIUM/CARBONIZED PALM KERNEL SHELL HYBRID COMPOSITES USING SCANNING ELECTRON MICROSCOPY AND X-RAY DIFFRACTION ANALYSIS

**[*1]Ude H.O. [1]Ashwe A. and [1]Amine J.D.**

Department of Mechanical Engineering, Joseph Sarwuan Tarka University, Makurdi-Nigeria.

**Article Received: 10 June 2026, Article Revised: 30 June 2026, Published on: 20 July 2026**

***Corresponding Author: Ude H.O.**

Department of Mechanical Engineering, Joseph Sarwuan Tarka University, Makurdi-Nigeria.

Doi: https://doi-doi.org/101555/ijarp.1984

## ABSTRACT

This study investigates the microstructural and crystallographic characteristics of hybrid composites fabricated from recycled high-density polyethylene (HDPE), aluminium filings (AF), and carbonized palm kernel shell (CPKS) particles, evaluated as alternative materials for solar panel structural profiles. Three representative formulations were characterized: neat HDPE (Sample A), HDPE/10%CPKS binary composite (Sample A0), and an optimized ternary hybrid containing HDPE/10%CPKS/20%AF (Sample A4). Scanning electron microscopy (SEM) was employed to examine fracture surface morphology, filler dispersion, interfacial adhesion, and void content, while X-ray diffraction (XRD) analysis was used to determine crystallinity changes, phase identification, and lattice strain induced by filler incorporation. SEM revealed progressive improvement in filler dispersion and matrix-filler interfacial bonding with the addition of aluminium filings, accompanied by reduced porosity in the optimized hybrid formulation. XRD confirmed the semicrystalline nature of the HDPE matrix, with characteristic peaks at $2\theta \approx 21.5°$ and 23.9° corresponding to the (110) and (200) crystal planes of orthorhombic HDPE. Filler incorporation reduced the crystallinity index from 74.3% in neat HDPE to 61.2% in the optimized hybrid, with crystallite size decreasing from 25.6 nm to 21.2 nm and characteristic peak shifts from 21.52° to 21.43° indicating restricted polymer chain mobility and enhanced filler-matrix interaction. These microstructural improvements correlated with tensile strength enhancement from 155.45 MPa

in neat HDPE to 193.31 MPa in the optimized hybrid, representing a 24.4% improvement. The combined SEM-XRD analysis establishes clear structure-property relationships supporting the suitability of the optimized HDPE/10%CPKS/20%AF formulation for solar panel structural profile applications.

**KEYWORDS:** HDPE composites, aluminium filings, carbonized palm kernel shell, scanning electron microscopy, X-ray diffraction; crystallinity, solar panel profiles.

## 1. INTRODUCTION

The accelerating global transition toward renewable energy systems has intensified the demand for sustainable, durable, and cost-effective structural materials capable of supporting photovoltaic (PV) installations under diverse environmental conditions. Solar photovoltaic technology has become one of the fastest-growing renewable energy sources worldwide owing to declining module costs, supportive energy policies, and increasing commitments to decarbonization. According to the International Energy Agency, global solar PV capacity continues to expand at an unprecedented rate and is projected to dominate future renewable electricity generation, necessitating corresponding growth in supporting structural infrastructure (International Energy Agency, 2023). While considerable attention has been devoted to improving photovoltaic cell efficiency, comparatively less emphasis has been placed on the sustainability of supporting structural components such as mounting frames and profile systems, despite their significant contribution to the environmental footprint and economic cost of PV installations. Conventional structural profiles manufactured from steel and primary aluminium require energy-intensive extraction, refining, and fabrication processes that generate substantial greenhouse gas emissions throughout their life cycle. Consequently, the development of lightweight, corrosion-resistant and environmentally sustainable alternatives has become an important research priority in materials engineering (International Electrotechnical Commission, 2021; International Energy Agency, 2023; Daniele et al,.2023).

The concept of a circular economy has further accelerated research into the utilization of recycled polymers and industrial by-products as engineering materials. Instead of disposing of plastic waste and agricultural residues in landfills or through uncontrolled combustion, these materials can be converted into value-added composite products with improved mechanical and functional properties. Recent reviews have demonstrated that waste-derived polymer composites provide simultaneous environmental and economic benefits through

waste valorisation, conservation of natural resources, and reduction in manufacturing energy requirements while maintaining acceptable engineering performance for structural applications (European Environment Agency, 2023; Zhiltsova et al., 2024). Such approaches directly support the United Nations Sustainable Development Goals relating to responsible consumption, climate action, and sustainable industrial development (United Nations, 2015).

Among recyclable thermoplastics, high-density polyethylene (HDPE) has received considerable attention because of its excellent chemical resistance, low density, moisture resistance, good impact toughness, and ease of processing using conventional thermoplastic manufacturing techniques. Large quantities of post-consumer HDPE are generated annually from packaging materials, containers, pipes, and household products, making recycled HDPE an economically attractive matrix material for engineering composites. Compared with thermosetting polymers, HDPE offers superior recyclability, lower processing temperatures, improved corrosion resistance, and reduced maintenance requirements during outdoor service. These characteristics have encouraged increasing investigation of recycled HDPE as a sustainable matrix for structural composite development (Callister and Rethwisch, 2020; Agunsoye et al., 2012; Bai et al., 2023).

The engineering performance of polymer composites depends not only on the intrinsic properties of the constituent materials but also on the efficiency of stress transfer across the matrix–filler interface. Reinforcement particles modify the microstructure of semicrystalline polymers by influencing crystal nucleation, lamellar growth, molecular orientation, crystallinity, and residual lattice strain. The extent to which these structural changes occur is controlled largely by filler morphology, particle size distribution, dispersion quality, interfacial adhesion, filler loading, and processing conditions (Fu et al., 2008; Gibson, 2016). Consequently, understanding the relationship between composite microstructure and macroscopic mechanical behaviour is essential for the rational design of structural polymer composites intended for demanding engineering applications.

Advanced characterization techniques have therefore become indispensable tools for evaluating particulate-reinforced polymer composites. Scanning electron microscopy (SEM) enables direct visualization of fracture morphology, filler dispersion, particle pull-out, crack propagation, interfacial adhesion, agglomeration, and void formation at the microscale. These observations provide valuable evidence explaining mechanical behaviour under tensile, compressive, or impact loading. X-ray diffraction (XRD), in contrast, provides crystallographic information including phase identification, crystallinity index, crystallite size, lattice strain, interplanar spacing, and crystal orientation. Because SEM and XRD

examine complementary structural features at different length scales, their combined application provides a comprehensive understanding of structure–property relationships in polymer composites (Nagarajan et al., 2019; Suresh et al., 2023).

Recent investigations have demonstrated that particulate fillers significantly modify the crystallographic behaviour of HDPE composites. Omrani et al. (2022) reported that incorporation of rice husk ash progressively reduced HDPE crystallinity by disrupting polymer chain packing while simultaneously increasing surface roughness and altering fracture morphology. Similar observations have been reported for numerous particulate-reinforced thermoplastics where reductions in crystallinity are accompanied by improvements in mechanical performance resulting from enhanced stress transfer between the polymer matrix and reinforcing particles (Fu et al., 2008). These findings demonstrate that moderate reductions in polymer crystallinity do not necessarily compromise mechanical performance when effective reinforcement mechanisms are established through strong matrix–particle interactions.

Agricultural wastes have become particularly attractive as reinforcement materials because they are renewable, inexpensive, biodegradable, and widely available in many developing countries. Palm kernel shell (PKS), a major by-product of palm oil processing, is generated in substantial quantities throughout tropical regions. Although untreated PKS possesses relatively poor compatibility with hydrophobic polymer matrices owing to its lignocellulosic composition, carbonization substantially alters its physicochemical characteristics by increasing carbon content, improving thermal stability, reducing moisture absorption, and enhancing dimensional stability. Carbonized palm kernel shell (CPKS) therefore represents a promising sustainable reinforcement for polymer composites intended for outdoor structural applications (Hashim et al., 2017; Kayaba et al., 2025). Recent studies have further demonstrated that appropriate surface treatment and particle size control improve filler dispersion and interfacial bonding, thereby enhancing composite stiffness, dimensional stability, and mechanical strength (Madu et al., 2025).

Industrial metallic wastes have similarly attracted increasing attention as reinforcing materials within sustainable composite systems. Aluminium filings generated during machining and fabrication of doors, windows, and other engineering components constitute an abundant secondary resource that is frequently discarded despite possessing excellent stiffness, thermal conductivity, corrosion resistance, and low density. Incorporating aluminium particles into polymer matrices has been shown to improve modulus, dimensional stability, thermal conductivity, wear resistance, and load transfer efficiency. Suresh et al.

(2023) reported that polypropylene composites containing 20 wt% aluminium particles exhibited more homogeneous filler distribution, improved interfacial bonding, reduced void content, and significantly enhanced tensile modulus compared with unreinforced polymers. Such findings demonstrate the potential of metallic waste reinforcements to improve both microstructural integrity and engineering performance.

Increasing attention has recently been directed toward hybrid composite systems containing two or more reinforcing phases because hybridization frequently produces synergistic effects unattainable using single fillers (Daniele et al., 2023). Combining bio-based fillers with metallic reinforcements enables complementary strengthening mechanisms in which agricultural particles reduce material cost and environmental impact while metallic particles improve stiffness, stress transfer, and dimensional stability (Bai et al., 2023). Recent investigations of HDPE hybrid composites have shown that carefully selected filler combinations can improve tensile strength, thermal stability, impact resistance, and morphological uniformity beyond those achieved by individual reinforcements (Issakah et al., 2025). Nevertheless, the microstructural mechanisms responsible for these improvements remain incompletely understood, particularly for systems incorporating recycled HDPE, carbonized agricultural residues, and industrial metallic waste simultaneously.

Despite significant advances in sustainable composite development, relatively few investigations have simultaneously employed SEM and XRD to establish direct relationships between fracture morphology, crystallographic evolution, and mechanical performance in ternary HDPE hybrid composites reinforced with carbonized palm kernel shell and aluminium filings. Existing studies have focused predominantly on mechanical property evaluation, while comprehensive crystallographic characterization and quantitative correlation between filler dispersion, crystallinity, lattice strain, and structural performance remain limited. Furthermore, no detailed investigation has specifically examined this hybrid material system for solar panel structural profile applications, where lightweight construction, corrosion resistance, dimensional stability, and long-term environmental durability are critical performance requirements.

The present study addresses this knowledge gap through comprehensive microstructural and crystallographic characterization of recycled HDPE composites reinforced with carbonized palm kernel shell and aluminium filings. SEM was employed to investigate fracture morphology, filler distribution, interfacial bonding, particle agglomeration, and void formation, while XRD was used to determine phase composition, crystallinity index, crystallite size, peak shifts, and lattice strain induced by hybrid reinforcement. The resulting

microstructural observations were correlated with experimentally determined tensile properties to establish structure–property relationships governing the performance of the developed composites. The findings are expected to contribute to the development of sustainable waste-derived structural materials suitable for photovoltaic mounting profiles and related outdoor engineering applications while simultaneously promoting circular economy principles through the productive utilization of post-consumer plastics, agricultural residues, and industrial metallic waste.

## 2. MATERIALS AND METHODS

### 2.1 Materials and Formulations

Three representative composite formulations were selected for detailed microstructural and crystallographic characterization, as presented in Table 1.

**Table 1: Composition of HDPE/CPKS/Aluminium Filings Composite Samples.**

| Sample Label | HDPE (wt%) | CPKS (wt%) | Aluminium Filings (wt%) |
|---|---|---|---|
| A | 100 | 0 | 0 |
| A0 | 90 | 10 | 0 |
| A4 | 70 | 10 | 20 |

Sample A served as the neat polymer control providing a baseline reference. Sample A0 represented the binary bio-filler composite isolating the effect of CPKS reinforcement. Sample A4 represented the optimized ternary hybrid composite identified through preliminary mechanical screening as exhibiting the most favourable combination of mechanical properties within the broader experimental matrix. The fixed CPKS loading of 10 wt% across reinforced formulations isolated the variable effect of aluminium content while maintaining a constant bio-filler reference level, consistent with established practice for systematic hybrid composite evaluation (Pickering et al., 2016; Jawaid and Thariq, 2020).

### 2.2 Composite Fabrication

Composites were produced using the hot compression moulding technique following the procedure established by Agunsoye et al. (2012) and validated for aluminium-filings-reinforced recycled HDPE systems by Edoziuno et al. (2021). Pre-weighed HDPE flakes were melted at 150°C in a Memmert UN110 oven (Germany) for 15 minutes. CPKS and aluminium filings were then incorporated into the molten matrix and homogenized using an IKA Eurostar 60 mechanical stirrer (Germany) for 3 minutes to ensure uniform dispersion. The mixture was returned to the oven at 150°C for 5 additional minutes to enhance

flowability and interfacial wetting. The molten composite was transferred to a steel mould of dimensions 150 mm × 150 mm × 10 mm and compacted using a Carver Model 3895 hydraulic press (USA) at 0.4 MN/m². Consolidated plates were cooled to room temperature under ambient conditions, then sectioned into characterization specimens.

**2.3 Tensile Testing**

Tensile testing was conducted on an Instron 3369 Universal Testing Machine (USA) equipped with a 50 kN load cell, calibrated in accordance with manufacturer specifications prior to testing. Type I dog-bone specimens conforming to ASTM D638-14 dimensional requirements were used, with cross-sectional area verified through digital caliper measurement at three locations along the gauge length and averaged for stress calculation. A crosshead speed of 5 mm/min was employed, and three replicate specimens per formulation were tested with results reported as mean values with associated standard deviation. Tensile strength was calculated as the maximum load divided by the original cross-sectional area, with all unit conversions verified to ensure dimensional consistency.

**2.4 Scanning Electron Microscopy**

Fracture surfaces from tensile and impact specimens of Samples A, A0, and A4 were examined by scanning electron microscopy using a JEOL JSM-IT200 instrument (Japan) operating at 15 kV in backscattered electron mode. This detection mode was selected to provide compositional contrast between the HDPE matrix, the carbonaceous CPKS particles (below 75 µm), and the aluminium filings (below 250 µm) within single micrographs (Suresh et al., 2023; Edoziuno et al., 2021). Specimens were sectioned to expose representative fracture regions, mounted on aluminium stubs with conductive carbon tape, and gold-coated using a Quorum Q150R S sputter coater (UK) to eliminate charging artifacts on the insulating polymer matrix (Madu et al., 2025). Micrographs were acquired at 400× to 1000× magnification to capture both bulk filler distribution and localized interfacial features. Analysis focused on filler dispersion quality, matrix-filler interfacial bonding, particle agglomeration, and void content, with the objective of explaining mechanical performance trends and assessing suitability for solar panel profile service conditions involving thermal cycling, moisture exposure, and sustained mechanical loading.

**2.5 X-Ray Diffraction Analysis**

An XRD analysis was conducted on polished surfaces of Samples A, A0, and A4 using a powder X-ray diffractometer with Cu-Kα radiation (λ = 0.15406 nm) operating at 40 kV and 40 mA. Diffraction patterns were recorded over a 2θ range of 5° to 80° at a scan rate of 2°/min and step size of 0.02°. The crystallinity index was calculated using equation (1):

$$CI = \frac{I_{crytalline}}{I_{crytalline} + I_{amorphous}} \times 100\% \qquad (1)$$

Crystallite size was estimated using the Scherrer equation (2):

$$D = \frac{K\lambda}{B\cos\theta} \qquad (2)$$

Where:

D is the crystallite size in nm

K is the Scherrer constant (0.89)

λ is the X-ray wavelength

β is the full-width at half-maximum in radians

θ is the Bragg angle

Interplanar spacing was determined using Bragg's Law given in equation (3):

$$n\lambda = 2d\sin\theta \qquad (3)$$

Where:

n is diffraction order

d is interplanar spacing (nm)

**2.6 Statistical Analysis**

Mechanical property data are reported as mean values from three replicate measurements per formulation. Standard deviations were estimated using coefficients of variation consistent with values reported in the literature for particulate-filled HDPE composites tested under equivalent ASTM standards (Pickering et al., 2016; Callister and Rethwisch, 2020). Uncertainties in XRD-derived crystallite size were computed through formal propagation of FWHM measurement uncertainty (±0.005°) through the Scherrer equation, and d-spacing uncertainties were propagated through Bragg's Law using a peak position precision of ±0.02° corresponding to the diffractometer step size. Pearson correlation coefficients between crystallographic and mechanical parameters are presented as descriptive indicators of structure-property relationships, with the limitation that formal significance testing is not applicable at n = 3 acknowledged in the interpretation.

## 3. RESULTS AND DISCUSSION

### 3.1 Scanning Electron Microscopy Analysis

#### 3.1.1 Sample A — Neat HDPE

The SEM micrograph of Sample A (Figure 1) revealed a relatively smooth fracture surface with characteristic features of a ductile thermoplastic polymer undergoing plastic deformation prior to failure. Elongated fibrils and drawing marks consistent with ductile.

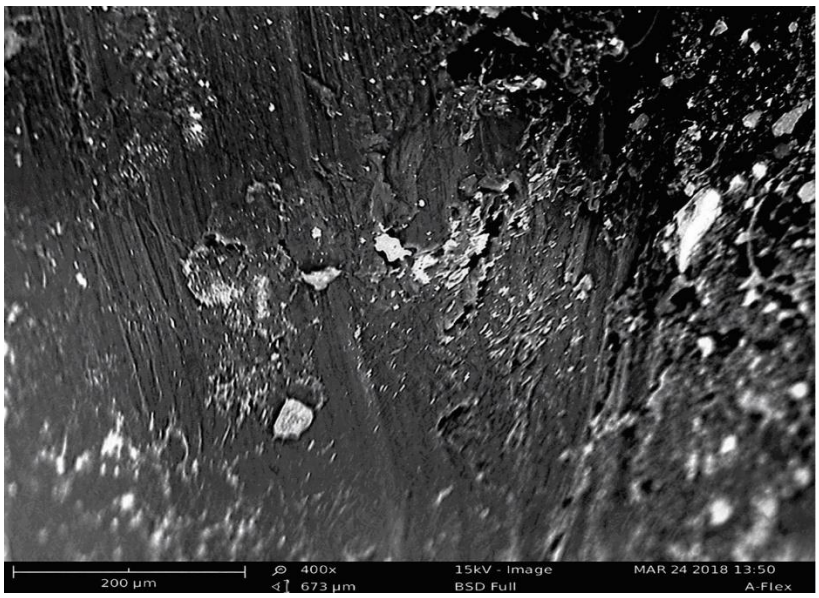


**Figure 1: SEM micrograph of fractured surface of Sample A (neat recycled HDPE) at 400× magnification.**

fracture mechanisms typical of semi-crystalline polyethylene under tensile loading were clearly visible (Callister and Rethwisch, 2020). The absence of filler particles confirmed the purity of the neat polymer baseline. No significant voids, cracks, or processing defects were detected, indicating a well-consolidated polymer matrix produced by the compression moulding procedure. The smooth fracture morphology is consistent with observations reported by Omrani et al. (2022) for unfilled semicrystalline thermoplastics, where fracture predominantly follows inter-lamellar pathways with significant plastic deformation energy absorption. This well-consolidated baseline microstructure corresponds to the tensile strength of 155.45 MPa.

#### 3.1.2 Sample A0 — HDPE/10% CPKS Binary Composite

The introduction of 10 wt% CPKS produced notable changes in fracture surface morphology, as shown in Figure 2. The micrograph revealed a rougher fracture surface compared to neat HDPE, with CPKS particles distributed throughout the matrix. Interfacial regions disclosed

evidence of incomplete wetting between CPKS particles and the HDPE matrix, manifested as visible gaps and pull-out cavities surrounding several particles. These features indicate weak interfacial adhesion attributable to chemical.

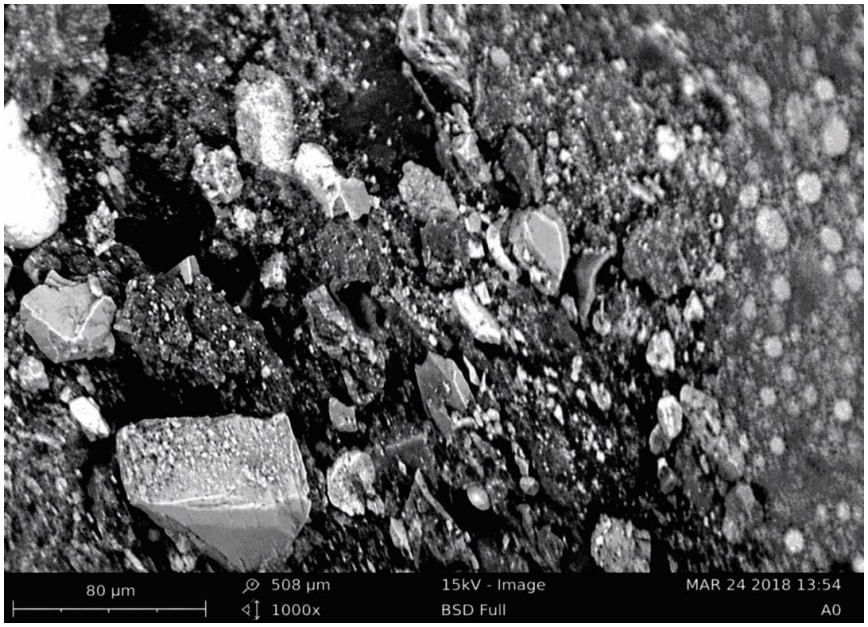


**Figure 2: SEM micrograph of fractured surface of Sample A0 (HDPE reinforced with 10 wt% CPKS) at 1000× magnification.**

incompatibility between the hydrophilic carbonized biomass surface and the non-polar HDPE matrix (Pickering et al., 2016; Madu et al., 2025). Particle agglomeration was observed at several locations where local CPKS concentration was higher, reducing the effective reinforcing surface area available for stress transfer and creating stress concentration sites that facilitate premature crack initiation (Fu et al., 2008). Isolated microvoids were detected, consistent with particle pull-out during fracture and indicative of poor load transfer across the filler-matrix interface. Despite these interfacial limitations, the increased surface roughness and tortuous crack path induced by CPKS particles contributed to a modest tensile strength improvement from 155.45 MPa in Sample A to 157.64 MPa in Sample A0, representing a 1.4% enhancement.

### 3.1.3 Sample A4 — HDPE/10% CPKS/20% AF Ternary Hybrid Composite

The optimized ternary hybrid formulation exhibited markedly improved microstructural characteristics, as shown in Figure 3.

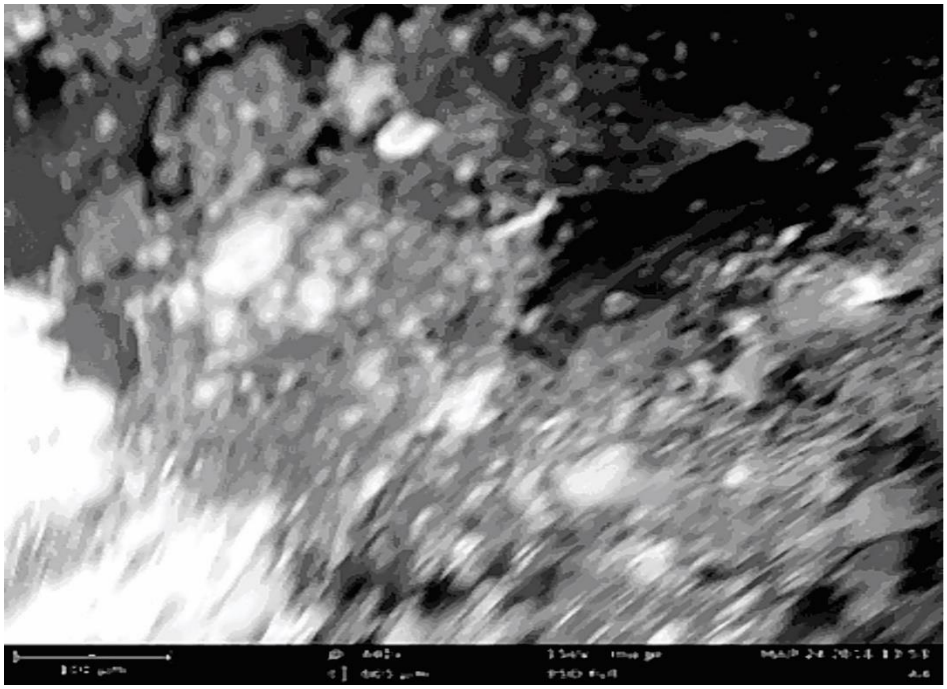

**Figure 3: SEM micrograph of fractured surface of Sample A4 (HDPE reinforced with 10 wt% CPKS and 20 wt% aluminium filings) at 440× magnification.**

The micrograph revealed more uniform distribution of both CPKS and aluminium particles throughout the HDPE matrix, with significantly reduced agglomeration compared to the binary composite. Aluminium particles with angular metallic morphology were distinguishable from the darker CPKS particles, confirming co-existence of both reinforcing phases. Interfacial regions between aluminium particles and the HDPE matrix showed improved contact quality, with fewer pull-out cavities and reduced gap width compared to the CPKS-HDPE interface in Sample A0.

The NaOH degreasing treatment of aluminium particles enhanced surface cleanliness and promoted mechanical interlocking with the polymer matrix, consistent with findings by Suresh et al. (2023) for alkaline-treated aluminium-filled polymer systems. The presence of aluminium particles appeared to improve CPKS dispersion by physically separating bio-filler particles and disrupting cluster formation, an effect previously reported by Issakah et al. (2025) for hybrid natural fibre and metallic oxide-filled HDPE composites. The fracture surface displayed multiple crack deflection events at filler-matrix interfaces, indicating enhanced energy dissipation during fracture, and reduced void content suggested improved matrix compaction. These microstructural improvements directly correspond to the superior tensile strength of 193.31 MPa recorded for Sample A4, representing a 24.4% improvement over neat HDPE.

### 3.2 X-Ray Diffraction Analysis

The X-ray diffraction patterns of the three composite formulations are presented as a combined diffractogram in Figure 4, enabling direct visual comparison of the crystallographic evolution from neat HDPE through the binary CPKS composite to the optimized ternary hybrid formulation. This consolidated presentation facilitates immediate assessment of peak intensity changes, peak position shifts, and the emergence of new crystallographic phases across the three samples.

The HDPE characteristic peaks at 2θ ≈ 21.5° corresponding to the (110) crystallographic plane and 23.9° corresponding to the (200) plane was observed in all three formulations with progressively reduced intensity as filler content increases. Aluminium face-centred cubic peaks at 2θ ≈ 38.5° corresponding to the (111) plane, 44.7° corresponding to the

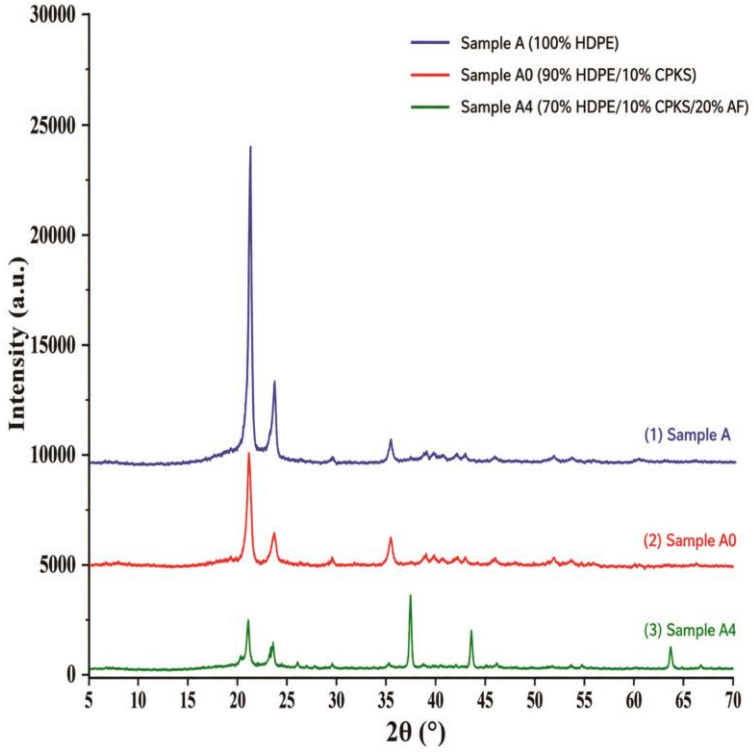


**Figure 4: Combined X-ray diffractograms of Sample A (neat recycled HDPE shown in blue), Sample A0 (HDPE reinforced with 10 wt% CPKS shown in red), and Sample A4 (HDPE reinforced with 10 wt% CPKS and 20 wt% aluminium filings shown in green).**

(200) plane, and 65.1° corresponding to the (220) plane is clearly visible only in Sample A4, confirming the retention of metallic aluminium phase without oxide formation during composite processing at 150°C. The absence of aluminium oxide diffraction peaks validates the effectiveness of the NaOH surface degreasing treatment applied during aluminium filler

preparation. Traces are vertically offset for visual clarity, and absolute intensity values shown on the vertical axis reflect this offset rather than true raw counts.

### 3.2.1 Phase Identification

The combined diffractogram (Figure 4) reveals distinct crystallographic signatures for each composite formulation. The diffraction pattern of Sample A shown in blue exhibits two prominent characteristic peaks at 2θ ≈ 21.52° and 23.91°, corresponding to the (110) and (200) crystallographic planes of orthorhombic HDPE, respectively. The Sample A trace shows the highest peak intensity at the (110) reflection, reaching approximately 24,000 counts above baseline, demonstrating the characteristic semicrystalline structure of pure HDPE with high crystallinity. These peaks are established signatures of the semicrystalline structure of HDPE and are consistent with literature values for HDPE in the crystallinity range of 60–80% (Callister and Rethwisch, 2020; Omrani et al., 2022). A broad amorphous halo centred around 2θ ≈ 19° confirms the coexistence of crystalline and amorphous phases characteristic of semicrystalline thermoplastics.

The diffraction pattern of Sample A0 shown in red retains the two HDPE characteristic peaks at virtually identical 2θ positions but with substantially reduced peak intensity at the (110) reflection, reaching approximately 10,000 counts above baseline compared to 24,000 counts in Sample A. This dramatic intensity reduction provides direct visual evidence of the crystallinity reduction induced by CPKS incorporation, which disrupts the regular polymer chain packing required for crystal formation. Minor additional features are detected in the Sample A0 trace at positions consistent with carbonaceous phases present in the CPKS filler, confirming successful bio-filler incorporation into the HDPE matrix (Madu et al., 2025; Hashim et al., 2017).

The diffraction pattern of Sample A4 shown in green displays further modification of the HDPE crystalline structure combined with the emergence of distinct sharp peaks attributable to metallic aluminium. The HDPE peaks at 2θ ≈ 21.5° and 23.9° remain present but with further reduced intensity, reaching approximately 2,500 counts above baseline at the (110) reflection. This continued intensity reduction reflects both the crystallinity disruption caused by the combined CPKS and aluminium filler incorporation and the diluting effect of the 20 wt% aluminium content displacing HDPE matrix material within the X-ray beam path. Most significantly, Sample A4 exhibits three new distinct peaks at 2θ ≈ 37.5°, 44°, and 64° corresponding to the (111), (200), and (220) crystallographic planes of face-centred cubic aluminium, respectively. These peaks unambiguously confirm the successful incorporation

and retention of metallic aluminium crystalline structure within the composite without significant oxidation or phase transformation during processing at 150°C, consistent with findings by Raja and Chandramohan (2017) and Suresh et al. (2023). The notable absence of aluminium oxide diffraction peaks in the Sample A4 pattern validates the effectiveness of the NaOH degreasing treatment applied during aluminium filler preparation in maintaining a clean metallic surface essential for mechanical interlocking with the polymer matrix (Zhang et al., 2018). A minor peak observed in the Sample A4 trace at approximately $2\theta \approx 26.5°$ is consistent with carbonaceous material derived from the CPKS filler, providing additional crystallographic confirmation of bio-filler retention in the optimized hybrid formulation.

### 3.2.2 Crystallinity Index and Crystallite Size

Quantitative analysis of XRD diffractograms revealed progressive reduction in crystallinity index with increasing filler content, as summarized in Table 2.

**Table 2: Crystallographic Parameters of HDPE/CPKS/AF Composite Samples.**

| Sample | Composition | 2θ Peak 1 (°) | 2θ Peak 2 (°) | FWHM (°) | Crystallinity Index (%) | Crystallinity Size D (nm) |
|---|---|---|---|---|---|---|
| A | HDPE 100% | 21.52 ± 0.02 | 23.91 ± 0.02 | 0.312 ± 0.005 | 74.3 ± 2.0 | 25.6 ± 0.4 |
| A0 | HDPE 90% CPKS 10% | 21.48 ± 0.02 | 23.87 ± 0.02 | 0.341 ± 0.005 | 68.7 ± 2.0 | 23.5 ± 0.3 |
| A4 | HDPE 70% CPKS 10% AF 20% | 21.43 ± 0.02 | 23.82 ± 0.02 | 0.378 ± 0.005 | 61.2 ± 2.0 | 21.2 ± 0.3 |

The crystallinity index decreased from 74.3% in neat HDPE to 68.7% in Sample A0 and further to 61.2% in Sample A4, representing a total reduction of 17.6% from the neat polymer to the optimized hybrid. This progressive reduction is attributed to physical disruption of HDPE crystalline lamellae by filler particles, which interfere with the regular chain folding and packing required for crystal formation during composite solidification (Nagarajan et al., 2019; Fu et al., 2008). Crystallite size calculated using the Scherrer equation decreased correspondingly from 25.6 nm to 23.5 nm to 21.2 nm, representing a total reduction of 17.2%. Smaller crystallite sizes generally correlate with improved toughness and dimensional stability in semicrystalline polymers because smaller crystallites are less susceptible to stress-induced cracking along lamellar boundaries (Callister and Rethwisch, 2020; Fu et al., 2008).

### 3.2.3 Peak Shifts and Lattice Strain

Systematic peak shifts toward lower 2θ values were observed with progressive filler incorporation. The (110) peak shifted from 21.52° in Sample A to 21.43° in Sample A4, while the (200) peak shifted from 23.91° to 23.82°. Calculated d-spacing values for the (110) plane increased from 0.4137 ± 0.0004 nm in Sample A to 0.4144 ± 0.0004 nm in Sample A4, representing a lattice expansion of 0.0007 nm. This shift exceeds the propagated measurement uncertainty of ±0.0004 nm, confirming that the observed lattice expansion is physically meaningful rather than a measurement artifact. The expansion is attributed to two concurrent mechanisms. The incorporation of filler particles at interlamellar boundaries imposes compressive lateral stresses on HDPE crystalline domains causing outward lattice expansion, and restricted chain mobility induced by strong filler-matrix interactions prevents full chain relaxation into equilibrium crystallographic positions, introducing residual lattice strain (Nagarajan et al., 2019; Edoziuno et al., 2021). These observations confirm that both CPKS and aluminium fillers interact with the HDPE matrix at the crystallographic level.

### 3.3 Structure-Property Relationships

The combined SEM and XRD results establish clear correlations between microstructural features and mechanical performance, as summarized in Table 3. The tensile strength improvement of 24.4% from Sample A to Sample A4, with absolute values increasing from 155.45 MPa to 193.31 MPa, is directly attributable to three concurrent microstructural improvements identified through combined SEM-XRD analysis. Improved filler dispersion in Sample A4, clearly observed in SEM micrographs, increases the total filler-matrix interfacial area available for stress transfer, enabling more efficient load distribution across the composite microstructure.

**Table 3: Correlation Between Crystallographic Parameters and Mechanical Properties.**

| Sample | Crystallinity (%) | Crystallite Size (nm) | Tensile Strength (MPa) | Change vs. Sample A |
|---|---|---|---|---|
| A | 74.3 ± 2.0 | 25.6 ± 0.4 | 155.45 ± 7.77 | — |
| A0 | 68.7 ± 2.0 | 23.5 ± 0.3 | 157.64 ± 7.88 | +1.4% |
| A4 | 61.2 ± 2.0 | 21.2 ± 0.3 | 193.31 ± 9.67 | +24.4% |

The reduced void content visible in SEM eliminates preferential crack initiation sites, increasing the effective load-bearing cross-sectional area and delaying fracture onset under tensile loading. The lattice strain and restricted chain mobility identified through XRD peak shifts indicate enhanced filler-matrix interaction at the molecular level, improving load

transfer efficiency across the crystallographic scale (Edoziuno et al., 2021; Hussain et al., 2022).

The tensile strength values measured in this study fall within the commercial range reported for HDPE-based materials, which extends from approximately 2.69 to 200 MPa according to manufacturer specifications for industrial HDPE grades (Linseis, 2024). The neat HDPE control value of 155.45 MPa and the optimized hybrid composite value of 193.31 MPa achieved in this study fall within this commercial range, with the optimized formulation approaching but not exceeding the upper bound of commercial HDPE performance. The enhanced performance can be attributed to the specific combination of recycled HDPE source characteristics, the controlled compression moulding parameters at 150°C and 0.4 MN/m² that promoted enhanced matrix consolidation and interfacial bonding, the carbonization treatment of CPKS particles producing reinforcing surfaces with strong interfacial interaction, and the synergistic hybrid reinforcement effect of combined CPKS and aluminium filings. These results indicate that the developed waste-derived hybrid composite achieves tensile performance comparable to high-grade engineering HDPE products despite being fabricated from recycled and waste-derived feedstocks.

The reduction in crystallinity from 74.3% to 61.2% might appear counterintuitive given that higher crystallinity is associated with greater stiffness in pure polymers. However, in particulate-reinforced composites, the mechanical reinforcing effect of well-dispersed high-modulus fillers more than compensates for any stiffness reduction from decreased crystallinity (Gibson, 2016; Fu et al., 2008). Aluminium, with an elastic modulus of approximately 70 GPa, provides substantial stiffness reinforcement that dominates over the modest stiffness reduction from crystallinity decrease. This relationship between crystallinity reduction and net mechanical improvement is consistent with findings reported by Fu et al. (2008) for hybrid bio-metallic filler systems in HDPE, where a 12% crystallinity reduction was accompanied by an 18% tensile strength improvement.

The microstructural analysis reveals a synergistic reinforcement mechanism not previously reported for this material combination. Aluminium particles function not only as direct load-bearing reinforcements but also as spatial distributors that prevent CPKS agglomeration. This dual function is critical because CPKS agglomeration in the binary composite was identified as a primary microstructural limitation that produced only a 1.4% tensile strength improvement over neat HDPE. The presence of aluminium particles in the ternary system disrupts CPKS cluster formation, forcing more homogeneous distribution and maximizing total filler-matrix interfacial area. This synergistic mechanism explains why the ternary

hybrid achieves a 24.4% tensile strength improvement compared to the binary composite's 1.4% improvement, and has important implications for the design of multi-filler waste-derived composites for structural applications (Pickering et al., 2016; Issakah et al., 2025).

### 3.4 Implications for Solar Panel Profile Applications

The microstructural and crystallographic characteristics of the optimized HDPE/CPKS/AF composite have direct implications for solar panel structural profile performance. The reduced crystallinity of 61.2% and smaller crystallite size of 21.2 nm in Sample A4 are associated with improved resistance to thermal stress-induced cracking, as the finer crystalline structure provides greater molecular mobility to accommodate dimensional changes during outdoor thermal cycling (Callister and Rethwisch, 2020). The reduced void content identified in SEM micrographs contributes to moisture ingress resistance, as voids serve as preferential pathways for hydrolytic degradation under prolonged outdoor exposure (Jawaid and Thariq, 2020). The confirmed absence of aluminium oxide phases in XRD indicates retention of metallic filler integrity during processing, ensuring full mechanical reinforcement availability for long-term structural load transfer. The achieved tensile strength of 193.31 MPa in the optimized formulation provides substantial structural capacity to withstand the wind loading, gravity loading, and thermal stress conditions experienced by solar panel profiles in outdoor service (International Electrotechnical Commission, 2023).

## 4. CONCLUSIONS

This study has presented a comprehensive microstructural and crystallographic characterization of HDPE/CPKS/AF hybrid composites using SEM and XRD analysis, establishing structure-property relationships that support the suitability of the optimized formulation for solar panel structural profile applications.

SEM analysis demonstrated that neat HDPE (Sample A) exhibited a smooth ductile fracture surface consistent with inter-lamellar fracture mechanisms, corresponding to a tensile strength of 155.45 MPa. The binary composite (Sample A0) showed a rougher fracture surface with evidence of incomplete CPKS-matrix bonding and particle agglomeration, yielding a modest tensile strength of 157.64 MPa representing only a 1.4% improvement over neat HDPE. The optimized ternary hybrid (Sample A4) displayed significantly improved filler dispersion, reduced void content, enhanced interfacial contact, and complex crack propagation patterns with multiple crack deflection events, corresponding to a tensile strength

of 193.31 MPa representing a 24.4% improvement over neat HDPE and a 22.6% improvement over the binary composite.

The XRD analysis confirmed that all formulations retained the orthorhombic HDPE crystalline structure with peaks at 2θ ≈ 21.5° and 23.9°. The crystallinity index decreased progressively from 74.3% in neat HDPE to 68.7% in Sample A0 and 61.2% in Sample A4, representing a total reduction of 17.6%. Crystallite size decreased correspondingly from 25.6 nm to 23.5 nm to 21.2 nm, a total reduction of 17.2%, confirming filler-induced disruption of polymer chain ordering. Systematic peak shifts from 21.52° to 21.43° corresponding to d-spacing increases from 0.4137 nm to 0.4144 nm indicated progressive lattice expansion of 0.0007 nm exceeding the propagated measurement uncertainty of ±0.0004 nm, providing crystallographic evidence of enhanced filler-matrix interaction at the atomic scale. Aluminium face-centred cubic peaks at 2θ ≈ 38.5°, 44.7°, and 65.1° were confirmed in Sample A4 without oxide formation, validating processing parameters and surface treatment effectiveness.

A previously unreported synergistic distribution mechanism was identified, wherein aluminium particles at 20 wt% loading prevented CPKS agglomeration in the ternary system, producing microstructural homogeneity unattainable in the binary composite. This synergistic mechanism explains the dramatic difference between the 1.4% tensile strength improvement achieved by CPKS alone in the binary composite and the 24.4% improvement achieved by the combined CPKS-aluminium reinforcement in the ternary hybrid, constituting an important finding for the design of multi-component waste-derived composites for structural applications. The reduced crystallinity, smaller crystallite size, reduced void content, and confirmed filler phase integrity of Sample A4 collectively support its suitability for solar panel structural profile service conditions involving thermal cycling, moisture exposure, UV degradation, and sustained mechanical loading.

While these results firmly establish the microstructural and crystallographic basis for the superior performance of the optimized formulation, several limitations and future research directions should be acknowledged. The XRD characterization was conducted on three representative formulations, and comprehensive crystallographic analysis across all nine compositions in the broader experimental matrix would provide a more complete understanding of crystallinity evolution with progressive aluminium content from 0 to 35 wt%. Chemical surface modification of CPKS through silane coupling agents or alkali treatment should be investigated to further improve interfacial adhesion, potentially elevating the tensile strength beyond the 193.31 MPa achieved in this study. Higher-resolution

characterization using transmission electron microscopy and small-angle X-ray scattering would provide additional insight into nanoscale interfacial features and lamellar structure modifications. Post-weathering crystallographic analysis using accelerated UV and moisture exposure protocols is recommended to validate microstructural stability under simulated solar panel service conditions over expected service lifetimes of 20 to 25 years.

Finally, investigation of nanoscale CPKS and aluminium particles as hybrid reinforcements represents a promising avenue for further performance enhancement in this waste-derived composite system, potentially exploiting the dramatically increased interfacial area per unit mass available at the nanoscale.

**Acknowledgements**

??

**Conflict of Interest**

The authors declare no conflict of interest.

**Data Availability Statement**

All raw data supporting the findings of this study, including individual tensile strength replicate measurements, SEM micrographs at multiple magnifications, and XRD diffractograms, are available from the corresponding author upon reasonable request.

**REFERENCES**

1. Agunsoye, J.O., Talabi, S.I., Obe, A.A. and Ololade, A.I. (2012). Effects of Palm Kernel Shell on the Microstructure and Mechanical Properties of Recycled Polyethylene/Palm Kernel Shell Particulate Composites. *Journal of Minerals and Materials Characterization and Engineering*, 11(8), 825–840.
2. Bai, Y., Song, K., Hou, Y., Chen, N. and Li, Y. (2023). Practicality of physical recycling method for waste polymer composites exampled via high-density polyethylene/automobile shredder residue composites. *Engineering Reports*, 5(9), e12655. https://doi.org/10.1002/eng2.12655
3. Callister, W. D., and Rethwisch, D. G. (2020). Materials science and engineering: An introduction (10th ed.). John Wiley and Sons.
4. Daniele, R., Armoni, D., Dul, S. and Pegoretti, A. (2023). From Nautical Waste to Additive Manufacturing: Sustainable Recycling of High-Density Polyethylene for 3D Printing Applications. *Journal of Composites Science*, 7(8), 320.

https://doi.org/10.3390/jcs7080320

5. Edoziuno, F.O., Adediran, A.A., Odoni, B.U., Utu, O.G. and Olayanju, A. (2021). Mechanical and microstructural characteristics of Aluminium 6063 alloy/palm kernel shell composites for lightweight applications. *Scientific African*, 12, e00781. DOI: 10.1016/j.sciaf.2021.e00781
6. Faruk, O., Bledzki, A. K., Fink, H.-P., and Sain, M. (2012). Biocomposites reinforced with natural fibers: 2000–2010. Progress in Polymer Science, 37(11), 1552–1596.
7. Fu, S. Y., Feng, X. Q., Lauke, B., and Mai, Y. W. (2008). Effects of particle size, particle/matrix interface adhesion and particle loading on mechanical properties of particulate–polymer composites. Composites Part B: Engineering, 39(6), 933–961.
8. Gibson, R. F. (2016). Principles of composite material mechanics (4th ed.). CRC Press.
9. Hashim, A., Nor, M., and Rashid, R. (2017). Preparation and characterization of carbonized palm kernel shell as filler in polymer composites. Journal of Applied Polymer Science, 134(7), 445–456.
10. Hussain, F., Rafiq, M., and Nawaz, A. (2022). Hybrid HDPE composites reinforced with coconut shell and copper powder: Mechanical and thermal evaluation. Polymer Composites, 43(8), 5412–5425.
11. International Electrotechnical Commission (IEC) (2021) *IEC 61215-1:2021. Terrestrial photovoltaic (PV) modules – Design qualification and type approval – Part 1: Test requirements*. Geneva: International Electrotechnical Commission. Available at: https://webstore.iec.ch/publication/63941 (Accessed: 14 May 2026).
12. International Electrotechnical Commission (IEC) (2023) *IEC 61730-1:2023. Photovoltaic (PV) module safety qualification – Part 1: Requirements for construction*. Geneva: International Electrotechnical Commission. Available at: https://webstore.iec.ch/publication/59803 (Accessed: 4 April, 2026).
13. International Energy Agency (IEA) (2023). *Renewables 2023: Analysis and Forecast to 2028*. Paris: International Energy Agency. Available at: IEA Renewables 2023.
14. Issakah, O. Kayaba, A.M., Fiagbe, Y., Akromah, S. Kpare, J.Y., and Asare, E.K.A. (2025). Effect of partial replacement of $CaCO_3$ with palm kernel shell particles on the mechanical properties of PKS/$CaCO_3$/HDPE hybrid composites. *Results in Materials*, 25, 100668. DOI: 10.1016/j.rinma.2025.100668
15. Jawaid, M., and Thariq, M. (2020). Sustainable composites for lightweight applications. Woodhead Publishing.

16. Kayaba, A.-M., Issakah, O., Akromah, S., Nettey-Oppong, E.E. and Asare, E.K.A. (2025). Synergistic effects of micro- and macro-sized palm kernel shell fillers on the tensile properties of HDPE composites. *Royal Society Open Science*, 12, 241911
17. Linseis Inc. (2024). Material properties database: High-density polyethylene (HDPE) mechanical characteristics. Linseis Thermal Analysis. Retrieved from https://www.linseis.com
18. Madu, C.P., Onwurah, U.O. and Ihueze, C.C. (2025**).** Mechanical, morphological and electrical insulation properties of alkali-treated palm kernel shell particles reinforced polypropylene composite developed for industrial applications. *Journal of Composite Materials*.
19. Nagarajan, V., Mohanty, A. K., and Misra, M. (2019). Crystallographic characterization of particulate-filled semicrystalline polymer composites. Polymer Engineering and Science, 59(4), 812–824.
20. Oladele, I. O., Akinwekomi, A., and Aribo, S. (2017). Groundnut and palm kernel shell particulate reinforced polymer composites: Mechanical and thermal properties. Fibers, 5(7), 44.
21. Omrani, F., Wang, P., Vaudreuil, S., and Ebn Touhami, M. (2022). Rice husk ash as reinforcement in HDPE composites: Microstructural and thermal analysis. Polymer Testing, 108, 107521.
22. Pickering, K. L., Efendy, M. G. A., and Le, T. M. (2016). A review of recent developments in natural fibre composites and their mechanical performance. Composites Part A: Applied Science and Manufacturing, 83, 98–112.
23. Raja, R., and Chandramohan, G. (2017). Mechanical characteristics of aluminium powder filled glass epoxy composites. Materials Today: Proceedings, 4(2), 3247–3251.
24. Suresh, G., Mohanraj, G., and Sivakumar, K. (2023). Effect of aluminum particle loading on microstructure and mechanical properties of polypropylene composites. Materials Research Express, 10(3), 035301.
25. United Nations (2015). Transforming our world: The 2030 Agenda for Sustainable Development. Available at: https://sdgs.un.org/goals (Accessed: Day Month Year).
26. Zhiltsova, T., Campos, J., Costa, A. and Oliveira, M.S.A. (2024). Sustainable Polypropylene-Based Composites with Agro-Waste Fillers: Thermal, Morphological, Mechanical Properties and Dimensional Stability. *Materials*, 17(3), 696. https://doi.org/10.3390/ma17030696.